JCI The Journal of Clinical Investigation

SPNS1 variants cause multi-organ disease and implicate lysophospholipid transport as critical for mTOR-regulated lipid homeostasis

Menglan He, … , Federico Torta, David L. Silver

J Clin Invest. 2025. https://doi.org/10.1172/JCI193099.

Research In-Press Preview Cell biology Metabolism

Graphical abstract

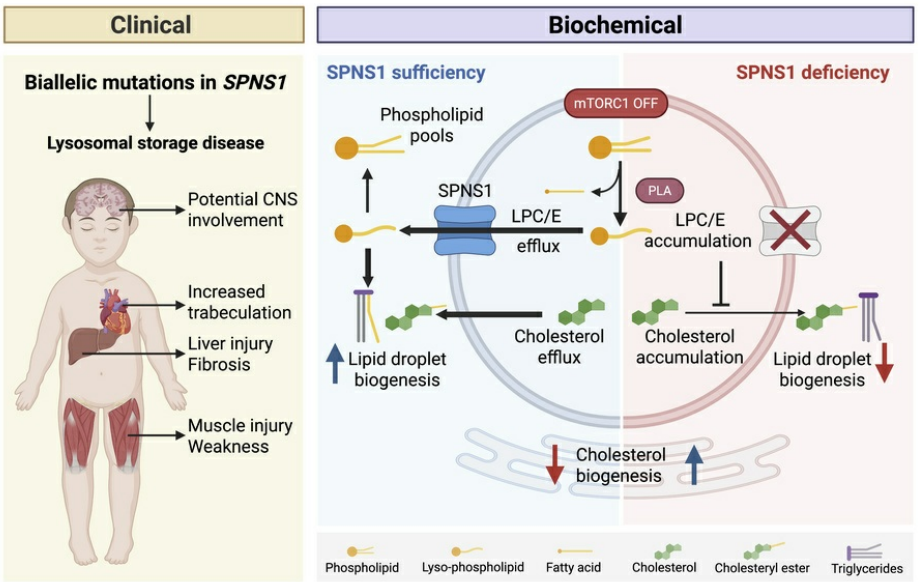

Title: *SPNS1* variants cause multi-organ disease and implicate lysophospholipid transport as critical for mTOR-regulated lipid homeostasis

Authors

Menglan He[1], Mei Ding[2,3], Michaela Chocholouskova[2,3], Cheen Fei Chin[1], Martin Engvall[4, 5], Helena Malmgren[5,6], Matias Wagner[7], Marlen C Lauffer[8], Jacob Heisinger[9], May Christine V Malicdan[10], Valerie Allamand[11,12], Madeleine Durbeej[12], Angelica Delgado Vega[5,6], Thomas Sejersen[13,14,15], Ann Nordgren[5,6,16,17], Federico Torta[1,2,3], David L Silver[1]

Affiliation

[1] Signature Research Program in Cardiovascular and Metabolic Disorders, Duke-National University of Singapore (NUS) Medical School, Singapore.

[2] Singapore Lipidomics Incubator (SLING), Life Sciences Institute, National University of Singapore, Singapore

[3] Precision Medicine Translational Research Programme and Department of Biochemistry, YLL School of Medicine, National University of Singapore, Singapore

[4] Centre for Inherited Metabolic Diseases, Karolinska University Hospital, Stockholm, Sweden

[5] Department of Molecular Medicine and Surgery, Karolinska Institutet, Stockholm, Sweden

[6] Department of Clinical Genetics and Genomics, Karolinska University Hospital, Solna, Stockholm, Sweden.

[7] Institute of Human Genetics, Klinikum Rechts der Isar, School of Medicine, Technical University of Munich, Munich, Germany; Institute for Neurogenomics, Helmholtz Zentrum München, Neuherberg, Germany; Division of Paediatric Neurology, Developmental Neurology, and Social Pediatrics, Dr von Hauner Children's Hospital, Munich, Germany.

[8] Dutch Center for RNA Therapeutics, Department of Human Genetics, Leiden University Medical Center, Leiden, The Netherlands.

[9] Hospital of the Brothers of Mercy Eisenstadt, Eisenstadt, Austria.

[10] National Institutes of Health Undiagnosed Disease Program, National Human Genome Research Institute, National Institutes of Health, Bethesda, MD, USA; Human Biochemical Genetics Section, Medical Genetics Branch, National Human Genome Research Institute, National Institutes of Health, Bethesda, MD, USA.

[11] Sorbonne Université, Inserm, Institut de Myologie, Center de Recherche en Myologie, Paris, France

[12] Department of Experimental Medical Science, Lund University, Lund, Sweden

[13] Department of Women´s and Children´s Health, Karolinska Institutet

[14] Department of Child Neurology, Karolinska University Hospital, Astrid Lindgren Children's Hospital, Stockholm, Sweden

[15] Center for Neuromusculoskeletal Restorative Medicine, Hong Kong Science Park, Shatin, New Territories, Hong Kong

[16] Department of Laboratory Medicine, Institute of Biomedicine, University of Gothenburg.

[17]Department of Clinical Genetics and Genomics, Sahlgrenska University Hospital, Gothenburg, Sweden.

Correspondence information

David L. Silver, Email: david.silver@duke-nus.edu.sg, Address: Duke-NUS Medical School, 8 College Road, Singapore 169857

Conflict of Interest statement

The authors have declared that no conflict of interest exists

Abstract:

SPNS1 is a lysosomal transporter mediating the salvage of lysoglycerophospholipids, the degradative products of lysosomal phospholipid catabolism. However, a role of lysolipid transport and salvage in regulating cellular lipid homeostasis and in disease is lacking. Here, we identified two families with biallelic *SPNS1* loss-of-function variants that presented primarily with progressive liver and striated muscle injury. Patient fibroblasts accumulated lysophospholipids including lysoplasmalogens and cholesterol in lysosomes with reduced cellular plasmalogens. Notably, SPNS1 deficiency resulted in reduced biogenesis of cytosolic lipid droplets containing triglycerides and cholesteryl esters. Mechanistically, we found that lysophospholipids transported by SPNS1 into the cytosol quantitatively contributed to triglyceride synthesis while lysosomal buildup of lyso-ether-phospholipid inhibited lysosomal cholesterol egress, effects that were enhanced with inhibition of mTOR. These findings support a gene-disease association and reveal connectivity between lysosomal transport of lysophospholipids and storage of reserve cellular energy as triglyceride and in the regulation of cholesterol homeostasis, processes that become important under nutrient limitation.

Main text

Introduction:

Lysosomes are degradative organelles that receive macromolecules from endocytosis, autophagy and phagocytosis. In addition to protein degradation leading to amino acid recycling, lysosomes also break down lipids and transport these back into biosynthetic pathways in the cytoplasm. One of the most highly understood lysosomal lipid transport pathways is the transport of cholesterol by the NPC1 and NPC2 proteins (1, 2). Biallelic loss of either NPC1 or NPC2 leads to Niemann-Pick disease type C (NPC), a lysosomal storage disease affecting multiple organs such as brain, liver, and spleen that is associated with lysosomal accumulation of cholesterol and sphingolipids (3-5). Cholesterol transport from lysosomes distributes to the plasma membrane and acts to negatively regulate *de novo* cholesterol biosynthesis in the endoplasmic reticulum (ER) by suppressing the processing of SREBP2, the master regulator of cholesterogenic gene expression (6, 7). Thus, cholesterol egress from lysosomes is critical for regulating cellular cholesterol homeostasis and a defect in this process is thought to be the major driver for NPC disease. In addition to lysosomal cholesterol egress, the glycerophospholipids phosphatidylcholine (PC) and phosphatidylethanolamine (PE) are the main lipid components of cellular membranes that continuously traffic through lysosomes. Within the lysosomal lumen PC and PE are degraded by phospholipases such as PLA2G15 to release lyso-phosphatidylcholine (LPC), lyso-phosphatidylethanolamine (LPE) and fatty acids (8, 9). Because of the zwitterionic nature of LPC and LPE lipids, we predicted that their egress out of lysosomes would require a transporter (10). Indeed, we and other groups identified SPNS1, a ubiquitously expressed lysosomal transmembrane protein belonging to major facilitator superfamily, as a proton-dependent transporter for LPC and LPE (10-12). We demonstrated that LPC transported out of lysosomes was re-acylated in the ER, constituting a lysosomal salvage pathway for phosphatidylcholine. SPNS1-mediated phospholipid salvage becomes essential for cell growth and survival under conditions of choline deficiency or blockade in cellular choline

uptake (12, 13), providing further evidence for the importance of the SPNS1/LPC salvage pathway in cellular physiology. Spns1 deficiency in mice is embryonic lethal, while knockdown or genetic deletion of *Spns1* in adult mice resulted in pathologies including liver inflammation, demyelination in brain and skeletal muscle atrophy (10, 11, 14, 15). Such pathological changes are associated with enlarged lysosomes and impaired autophagy, similar to the zebrafish models of SPNS1 deficiency(10, 11, 16, 17). The role of SPNS1 in human health and disease is less clear. A recent report identified three patients from one family with a homozygous variant of *SPNS1* (c.C884T:p.P295L) that presented with neurodevelopmental delay(11), but without reported liver or muscle pathologies. A direct link between this variant and cellular accumulation of LPC and LPE was not reported. Therefore, our understanding of the importance of *SPNS1* in human physiology is limited by lack of definitively identified pathogenic variants of *SPNS*1 that lead to human disease.

In addition to LPC and LPE, sphingolipid metabolites including hexosylceramides and sphingosine also accumulated in lysosomes of mouse models of Spns1 deficiency(10, 11). Notably, in liver-specific knockdown of *Spns1*, we found an increase in lysosomal levels of cholesterol -biochemical phenotypes reminiscent of NPC disease. The accumulation of lipids not transported by SPNS1 suggested that lysosomal accumulation of LPC and LPE can potentially affect the homeostasis of other lipids in the cells. Mechanistic/mammalian target of rapamycin(mTOR) is a key nutrient sensor that responds to growth hormone, insulin and lysosomal amino acid flux to regulate anabolic processes such as protein translation and lipogenesis (18-20). Recently, inhibition of mTOR has been shown to additionally regulate lysosomal phospholipid catabolism to produce LPC and fatty acids, the latter of which was demonstrated to contribute to the synthesis of cytosolic triglyceride lipid droplets (LD) as an adaptation to nutrient deficiency (21). However, the contribution of lysosomal LPC to cellular lipid homeostasis in conditions of mTOR inhibition remains unknown.

In this study we expand upon the clinical and mutational spectrum of *SPNS1*-associated disease and determine underlying mechanisms by which SPNS1 deficiency can negatively affect lysosomal and cellular lipid homeostasis.

Results

Biallelic *SPNS1* loss-of-function variants lead to a multiorgan disease

Family A:

The proband (A.II.1, male, 16 years old, Supplemental Figure 1A) and his younger brother (A.II.2, male, 8 years old) both presented with prolonged, transient neonatal unconjugated hyperbilirubinemia followed by persistently elevated transaminases, serum creatine kinase and myoglobin levels since 6 months and 12 months of age, respectively. There was no family history of liver, muscle or other metabolic disorders. Echocardiography showed increased trabeculation of the left ventricle in both brothers and discrete left ventricular hypertrophy in the proband. Motor milestones were achieved in the lower part of the normal spectrum in both brothers. At 4 years of age, gross motor function was slightly impaired in the proband, with calf pain and reduced ankle range of motion. At his last gross motor assessment at the age of 15 years, mild proximal/axial weakness was noted, particularly in the abdomen and upper extremities. He scored 93/96 on the Motor Function Measure but was unable to perform push-ups and could only do a few sit-ups with great difficulty. Both brothers are ambulatory but easily fatigued. Speech development was slightly delayed in both brothers. The proband was diagnosed with Attention Deficit Disorder at the age of 13 years. Neuropsychological assessments of cognition using the Wechsler Intelligence Scale for Children at 8 and 13 years of age showed average verbal abilities but reduced nonverbal abilities. Key clinical and laboratory findings are summarized in Supplemental Table 1.

Whole genome sequencing and analysis of the two affected brothers and their parents showed that the siblings both were compound heterozygous for two variants in the *SPNS1*-gene (NM_032038); c.(1247C>G), p[Ser416Cys] (referred as S416C) and c.(143_146dup),

p[Ile50Alafs*48] (referred as 143_146 dup). The father was the heterozygous carrier of the c.1247C>G variant, and the mother was the heterozygous carrier of c.143_146dup variant in the *SPNS1* gene. Two healthy sisters did not harbour any of the variants in the *SPNS1* gene. In addition, a hemizygous variant in the *PRDX4* gene was detected in both patients, and the mother was heterozygous carrier for this variant. However, this candidate gene was excluded as the healthy grandfather of the patients was hemizygous for this variant.

Family B:

We screened our in-house database(22) comprising >20,000 exome datasets for individuals with biallelic variants in *SPNS1* and identified patient 3 who is homozygous for the variant NM_032038.3:c.860C>T, p.(Thr287Met). Patient 3 is an 8-year-old male was born to consanguineous parents and presented with elevated transaminase and failure to thrive at 2.5 years of age. The liver transaminase, lactate dehydrogenase and serum creatine kinase had been persistently remained elevated. He was diagnosed with global development delay at 3 years old. He had neonatal cardiac abnormalities including cardiomegaly, large coronary arteries and small aortic isthmus but subsequent cardiac ultrasound had inconspicuous findings. Key clinical and laboratory findings are summarized in Supplemental Table 1.

SPNS1 variants result in loss-of-function of LPC transport

To understand the functional impact of the *SPNS1* variants identified in the patients, we introduced the mutations encoding S416C, T287M and 143_146dup into the human cDNA of *SPNS1* and overexpressed these in HEK293 cells. S416C and T287M were expressed at a similar level as wild-type (WT) SPNS1 while the full length 143_146dup (dup fl) variant resulted in a poorly expressed protein migrating at a lower molecular weight (Figure 1A). This residual expression is possibly due to usage of an alternative start codon located 38bp downstream of original start codon that is predicted to result in a smaller protein (referred as dup 516aa) having a new N-terminal sequence (Supplemental Figure 1, B and C), consistent with the smaller molecular weight detected by Western blot analysis (Figure 1A). In fact, when we

overexpressed the c.143_146dup variant having only the alternative start codon, the modified protein dup 516aa was expressed at a level similar to the WT SPNS1 (Figure 1A). In fibroblasts from patient A.II.1 and A.II.2, the protein level of SPNS1 was reduced compared to their age-matched controls (Figure 1, B and C). Such reduction is likely caused by the poor expression of the 143_146dup variant because the mother, who is the carrier of this variant, also had a similar reduction in SPNS1 protein level while the SPNS1 expression in father's fibroblasts was comparable to the age matched controls (Figure 1, B and C). To test the functionality of *SPNS1* variants, we used a cell surface LPC transport assay we previously developed, taking advantage of a cellular phenomenon that lysosomal membrane proteins traffic through the plasma membrane before entering the endocytic pathway(23). This assay works by overexpression of WT and variant constructs at the cell surface and quantifying uptake of [^{14}C]-LPC-oleate at an extracellular acidic pH to mimic the lysosomal environment. We first confirmed that S416C and T287M mutants were present at comparable levels as WT SPNS1 at the plasma membrane by immunofluorescence and cell surface biotinylation upon overexpression (Supplemental Figure 1, D and E). The plasma membrane level of the 143_146dup (dup fl) mutant was low, consistent with its poor cellular expression level (Supplemental Figure 1, D and E). We found that while cells overexpressing WT SPNS1 showed a dose-dependent uptake of [^{14}C]-LPC-oleate, the S416C and T287M variants had reduced transport activity (Figure 1, D and E), suggestive of a partial loss-of-function. In contrast, the dup fl variant showed reduced transport activity while the dup 516aa construct showed higher transport activity than WT (Figure 1F), indicating that the low transport activity of the dup fl variant is due to its poor expression. We also noticed that the transport activity of S416C and T287M variants was enhanced when the assay was performed at a lower pH (Figure 1G). This suggests that in the lysosome, where the luminal pH is close to 4.5, these mutants are partially functional. This is consistent with SPNS1 activity being pH dependent(10). To test the functionality of these two variants within the lysosome, we integrated cDNAs encoding WT, S416C and T287M into the *AAVS1* locus of HEK293T *SPNS1* KO cells. We confirmed that both variants were expressed at a similar level as WT SPNS1 (Supplemental

Figure 1F) and localized to lysosomes (Supplemental Figure 1G). The two patient variants were able to reduce the cellular LPC accumulation to a similar extent as WT SPNS1 (Supplemental Figure 1H). We also observed that the expression of S416C and T287M in the rescue cell lines were higher than endogenous SPNS1 expression in HEK293T (Supplemental Figure 1F), further supporting the conclusion that these *SPNS1* variants are partially active and their elevated expression in lysosomes can reduce LPC accumulation in SPNS1 KO cells. An examination of an AlphaFold predicted SPNS1 structure showed that Ser416 is located near the cytosolic end of the transport cleft, while Thr287 is in the transport cleft (Figure 1H). Both residues are highly conserved across the species (Supplemental Figure 1I) and expected to play a role in transport function through either direct substrate interactions or participating in conformational changes between the N- and C-terminal halves of SPNS1.

We similarly conducted biochemical analysis on the previously reported P295L variant of SPNS1(11). We found that P295L was expressed at a lower level than WT SPNS1 upon transient overexpression (Supplemental Figure 1J) and had minimal transport activity (Supplemental Figure 1, K and L). Notably, transiently overexpressed P295L exhibited mainly a reticular staining pattern and consequently had lower plasma membrane levels compared to WT SPNS1 as determined by cell surface biotinylation (Supplemental Figure 1, D and E), likely explaining its lack of transport activity in this assay and in the previous report (11). To determine the function of the P295L variant at the lysosome level, we similarly integrated the P295L variant into the *AAVS1* locus. In the rescued line, P295L localized to lysosomes and was expressed at a lower level than WT SPNS1 but at a similar level as endogenous SPNS1 (Supplemental Figure 1, F and G). Expression of P295L rescued LPC accumulation in *SPNS1* KO cells despite its lower expression as compared to WT SPNS1 (Supplemental Figure 1H). Taken together, these data suggested that P295L is functional in lysosomes but is poorly expressed.

To understand how *SPNS1* variants affect cellular lipid levels, we performed lipidomic analysis on patients and control fibroblasts from Family A. Consistent with a defect in exporting LPC

and LPE out of lysosomes, patient fibroblasts showed elevation of various species of LPC, LPE and lysophospholipids containing ether bonds including plasmalogens (Figure 1I). Notably, sphingosine and some of the hexosylceramide species were also elevated. The accumulation of these lysolipids were reversed by overexpressing SPNS1 (Figure 1J, Supplemental Figure 2A), supporting the conclusion that the accumulation of LPC and LPE in patient fibroblasts is dependent on the loss-of-function of *SPNS1*. Lipidomics profiling of patients' leukocytes from Family A peripheral blood revealed an increase in abundance of LPC, LPC-O/P and LPE level compared to their parents (Supplemental Figure 2B), which is consistent with the accumulation of lysophospholipids in the fibroblasts' samples (Figure 1I). On the other hand, the serum levels of LPC and LPC-O/P were reduced in patients, while level of hexoylceramides was elevated (Supplemental Figure 2C).

We previously showed that SPNS1 deficiency in HEK293T cells and liver resulted in enlarged LysoTracker positive compartments and accumulation of the autophagy marker LC3b-II(10). Consistent with *SPNS1* loss-of-function, *SPNS1* patient fibroblasts showed increased LysoTracker positive compartments (Figure 1, K and L) which could be due to increase in the number and size of lysosomes. Such phenotypic changes were reversed by overexpressing WT *SPNS1* in patient fibroblasts (Supplemental Figure 2, D and E). However, unlike in Spns1 deficient mouse liver, we did not observe an increase in basal levels of LC3b-II in patient fibroblasts as compared to their age-matched controls (Supplemental Figure 2F), suggesting that the *SPNS1* mutation p.Ser416Cys, which resulted in a partial loss-of-function (Figure 1D), caused a less severe impairment of lysosomal function as compared to complete absence of SPNS1 in cells (10).

SPNS1 deficiency results in impaired neutral lipid synthesis under mTOR inhibition

As an attempt to understand pathogenesis at the cellular level of the disease caused by *SPNS1* loss-of-function variants, we sought to investigate further the contribution of lysosomal lysophospholipid transport to cellular lipid homeostasis, an area that remains largely unexplored. Phospholipid catabolism in lysosomes has been shown to be essential for LD

biogenesis during nutrient deprivation and ER stress in various cell and animal models (24-26). mTOR has a central role in regulation of this process as it serves as a nutrient sensor that when inhibited results in increased delivery of membrane phospholipids to lysosomes (21). It was shown that lysosomal fatty acids derived from the catabolism of phospholipid drive triglycerides (TAG) synthesis which can either be used for β-oxidation or stored in LDs for future use (21, 27, 28). Therefore, phospholipid turnover in lysosomes and their recycling into cytosol is thought to provide an advantage to cell survival under stress. Because SPNS1 is essential for efflux of LPC out of lysosomes, we hypothesized that LPC transported by SPNS1 plays a role in neutral lipid, including TAG and cholesteryl ester (CE), storage processes when mTOR is inhibited. To test this idea, we treated WT and *SPNS1* KO HEK293T cell lines with Torin1, a specific mTORC1 inhibitor, and measured changes in cellular lipids over time using lipidomic analysis. As anticipated, LPC accumulated in *SPNS1* KO cells in a time dependent manner (Figure 2A). Strikingly, while WT cells were able to synthesize CE and TAG over time, *SPNS1* KO cells had greatly compromised ability to do so (Figure 2, B and C). This finding is further supported by the reduction in the number of BODIPY positive LD in *SPNS1* KO cell relative to WT cells (Figure 2, D and E). Similarly, while HBSS starvation of HeLa cell induced LD formation in WT cells, LD biogenesis was reduced in *SPNS1* KO cells (Supplemental Figure 3, A and B), indicating that the impairment of LD formation in *SPNS1* KO cells can be generalized to other forms of nutrient deprivation.

To assay the effect of SPNS1 deficiency on the efficiency of cellular TAG and CE synthesis, we utilized radioactive fatty acid tracing to measure diacylglycerol acyltransferase (DGAT) and acyl-coenzyme A:cholesterol acyltransferase (ACAT) activity, the rate-limiting enzymes in TAG and CE synthesis, respectively. After treating cells with Torin1 for 16 hrs, a trace amount of [^{14}C]-oleate was added to cells for another 4 hrs and labelled neutral lipid species were separated by thin layer chromatograph (TLC). *SPNS1* KO cell lines showed a reduction of [^{14}C]-oleate incorporated into TAG and CE (Figure 2F). The decrease in TAG synthesis could be either due to impaired DGAT enzymatic activity or reduced availability of acyl-CoA substrate.

We first ruled out the former by measuring DGAT activity in an isolated membrane fraction from *SPNS1* KO and WT cells. This DGAT activity assay indicated no significant difference in the rate of [^{14}C]-TAG formation from diacylglycerol (DAG) and [^{14}C]-oleoyl-CoA substrates in KO and WT cells in both basal and Torin1 treated conditions (Supplemental Figure 3, C and D). Since LPC accumulates inside lysosomes in *SPNS1* KO cells and LPC contains one covalently attached fatty acid, we reasoned that LPC that is transported out of lysosomes via SPNS1 could contribute its fatty acid for TAG synthesis. However, the existence of such crosstalk between LPC and TAG pools has not been previously demonstrated. To begin to test this concept, we added exogenous albumin-bound free fatty acid (FFA-18:1) or LPC-18:1 to bypass the lysosome and examine if this would rescue the defect in TAG synthesis in *SPNS1* KO cells. To directly deliver LPC to cytosolic membranes, we constructed a doxycline-inducible cell line expressing MFSD2A, a plasma membrane LPC transporter (29), or the transport-inactive mutant MFSD2A-D97A (30) in WT and *SPNS1* KO cells respectively (Figure 2G). Treatment with FFA-18:1 increased TAG synthesis in WT MFSD2A and mutant D97A cells, while LPC-18:1 treatment increased TAG synthesis only in cells expressing WT *MFSD2A* (Figure 2, H and I). Such a rescue effect of FFA-18:1 or LPC-18:1 supplementation was dose dependent (Supplemental Figure 3E). It is notable that the CE synthesis defect in *SPNS1* KO cells was not rescued by addition of LPC-18:1 or FFA-18:1 (Figure 2, H and J), indicating that a lack of fatty acid availability in the cytosolic compartment in *SPNS1* KO cells is not responsible for reduced CE synthesis. Taken together, these data indicate that lysosomal derived LPC does contribute to TAG synthesis and LD formation.

To provide an independent line of evidence that lysosomal derived LPC quantitively contributes to supplying fatty acid for TAG synthesis during mTOR inactivation, we conducted a stable isotope tracing study to follow the metabolic fate of PC delivered to the lysosome. Similar to our previously published experimental method, we complexed per-deuterated d82-1-palmitoyl-2-oleoyl-sn-glycero-3-phosphocholine (POPC) with apoE to form nanodiscs that are delivered to lysosomes thorough low-density lipoprotein receptor (LDLR) mediated

endocytosis (10). The use of d82-POPC allows us to trace all components (i.e. fatty acids, glycerol backbone and choline headgroup) of this PC into cellular lipids. Inside the lysosome, we anticipate that d82-POPC will be hydrolyzed to d49-LPC16:0 and d33-FFA18:1 by lysosomal PLA2 and to d51-LPC18:1 and d31-FFA16:0 by lysosomal PLA1. The LPC transported out of lysosomes via SPNS1 can be used directly for phosphatidylcholine synthesis or hydrolyzed further to release fatty acid (Figure 3A). Together with the fatty acid released directly from PC hydrolysis to LPC, these fatty acids could be utilized for phospholipid remodeling, DAG and TAG synthesis and β-oxidation (Figure 3A). As such, we quantified PC, TAG and DAG species that contain one or more of d33-18:1 fatty acyl chain, d31-16:0 fatty acyl chain, d5-glycerol backbone or d13-phosphocholine (Figure 3A).

Consistent with SPNS1 being a lysosomal LPC transporter, *SPNS1* KO cells accumulated d49-LPC16:0 and d51-LPC18:1(Figure 3, B and C). The higher level of d51-LPC18:1 than d49-LPC16:0 suggested that PLA1 activity might be more predominant than PLA2 activity in HEK293T cells. Consistent with our previous study that traced the fate of d9-choline in d9-1,2-dioleoyl-sn-glycero-3-phosphocholine (DOPC), *SPNS1* KO cells had reduced recycling of the glycerophosphocholine (GPC) headgroup into to PC pools (Figure 3B). We observed a 50% reduction of d51-LPC-18:1 or d49-LPC-16:0 containing PC generated from direct re-acylation of lysosomal-derived LPC by LPCAT activity in *SPNS1* KO cells (Figure 3D). Since d51-PC and d49-PC can undergo acyl chain remodeling through Land's cycle, we also observed a reduction in PC species containing only the deuterated GPC headgroup (d18-PC) in *SPNS1* KO cells (Figure 3E). Moreover, such LPC accumulation and deficiency of GPC headgroup salvage was exacerbated by Torin1 treatment (Figure 3, B-E), as mTOR inhibition can increase both endocytic delivery of lipid and lysosomal hydrolases activity (31, 32). These findings suggested that the SPNS1 mediated phospholipid salvage pathway is quantitatively important for maintaining cellular phospholipid homeostasis especially when mTOR activity is low.

We next quantified the fate of d31- and d33 fatty acyl groups in *SPNS1* KO and WT cells. WT cells increased the incorporation of d31-FA-16:0 and d33-FA-18:1 into TAG upon mTOR inhibition by 3-fold (Figure 3, B and F), confirming the ability of cells to utilize fatty acid derived from lysosomal phospholipid catabolism. In contrast, *SPNS1* KO cells had only slightly increased incorporation of d31-FA-16:0 and d33-FA-18:1 to TAG after Torin1 treatment (Figure 3B), resulting in a more than 50% reduction in TAG containing d33-FA-18:1 or d31-FA-16:0 when compared to WT cells under mTOR inhibition (Figure 3F). This finding is consistent with the 50% reduction in [^{14}C]-oleate labeling of TAG in our radioisotope tracing study (Figure 2I). On the other hand, d31-FA-16:0 and d33-FA-18:1 incorporation into PC (d31-PC and d33-PC) and DAG (d31-DAG, D33-DAG) was minimally affected by the absence of SPNS1 (Supplemental Figure 4, A and B), suggesting a preferential use of lysosomal derived fatty acids for maintaining PC and DAG levels. We noticed that in WT cells without mTOR inhibition, only 2.5% of d33-FA-18:1 and 4.8% of d31-FA-16:0 derived from d82-POPC was channeled for TAG synthesis, while this proportion increased to 6% and 11% respectively after Torin1 treatment (Supplemental Figure 4C). In contrast, we did not see such an increase of these labelled fatty acids in TAG in *SPNS1* KO cells (Supplemental Figure 4C). These findings support the existence of an adaptive shift in the fate of fatty acids derived from lysosomal LPC in response to changes in mTOR activity, and that this process is dependent on SPNS1-mediated LPC transport.

Deficiency of SPNS1 results in defective lysosomal cholesterol efflux

While the defect in TAG synthesis in *SPNS1* KO cells was rescued by supplementing cells with fatty acid or LPC, the defect in CE synthesis was not (Figure 2, H-J), suggesting that *SPNS1* KO cells have a deficiency in ER cholesterol or compromised ACAT activity. Cells acquire cholesterol thorough *de novo* synthesis and endocytosis of lipoproteins. NPC1 and NPC2 mediate the egress of low density lipoprotein (LDL) derived cholesterol out of lysosome(1, 2), and the lysosome-derived cholesterol first travels to the plasma membrane before trafficking to the ER, a process mediated by Aster proteins(33-35). We first examined

371 if ACAT activity was compromised in *SPNS1* KO cells by testing if enriching plasma membrane
372 cholesterol using methyl-beta cyclodextrin-cholesterol (MβCD) complex could rescue the CE
373 synthesis defect in *SPNS1* KO cells. Radioisotope tracing showed that both *SPNS1* KO and
374 WT cells were able to increase the incorporation of [^{14}C]-oleate into [^{14}C]-CE upon cholesterol
375 supplementation, indicating ACAT was functional in esterifying plasma membrane derived
376 cholesterol in *SPNS1* KO cells (Figure 4A). While KO cells synthesized 75% less [^{14}C]-CE
377 than WT cells under basal conditions, supplementation with cholesterol alone or with both
378 cholesterol and fatty acid only partially normalized the difference in CE synthesis as KO cells
379 synthesized 50% less [^{14}C]-CE than WT cells under these conditions (Figure 4A). This could
380 be due to a defect in either lysosomal egress or plasma membrane to ER trafficking of
381 cholesterol. The former would lead to a lysosomal accumulation of cholesterol while the latter
382 would lead to sequestration of cholesterol on plasma membrane. Therefore, we used
383 TopFluor^{TM}-cholesterol, a fluorescent cholesterol analog that can be esterified by fatty acids,
384 to metabolically labelled cellular cholesterol and visualize its subcellular localization after
385 Torin1 treatment. In WT cells, TopFluor^{TM}-cholesterol had a diffuse ER and PM staining pattern
386 that colocalized with LipidTOX^{TM} positive LDs after Torin1 treatment, indicating that
387 TopFluor^{TM}-cholesterol is channeled to cytosolic LDs (Figure 4B, Supplemental Figure 5A). In
388 contrast, *SPNS1* KO cells had a punctate pattern of TopFluor^{TM}-cholesterol that colocalized
389 with LysoTracker (Figure 4C), demonstrating that cholesterol delivered to cells using MβCD
390 accumulated in lysosomes of *SPNS1* KO. These findings likely explain the partial rescue of
391 CE synthesis in *SPNS1* KO cells treated with exogenously added cholesterol delivered by
392 MβCD (Figure 4A) as some of the cholesterols are sequestered in lysosome and not available
393 for acylation by ACAT.

394 To further examine the cellular distribution of endogenous cholesterol, cells were stained with
395 filipin, a fluorescent dye that specifically binds to unesterified cholesterol. We observed an
396 intracellular punctate staining pattern in *SPNS1* KO cells, while WT cells exhibited primarily
397 plasma membrane staining (Figure 4D). Such accumulation became more profound in Torin1

treated *SPNS1* KO cells (Figure 4, D and E) and was also observed in other cell types with SPNS1 deficiency, namely HeLa and HuH-7 cells (Supplemental Figure 5, B and C). As expected, there was a corresponding increase in cellular LPC levels in *SPNS1* KO HeLa or HuH-7 cells which was exacerbated with Torin1 treatment (Supplemental Figure 5D). We also developed a flow cytometry method to quantify intracellular filipin staining intensity. As more than 90% of free cholesterol is estimated to reside in the plasma membrane (36, 37), we used a short-term treatment of cells with MβCD to deplete plasma membrane cholesterol before staining with filipin (38), so that lysosomal filipin staining will be the primary signal being measured. We verified that our treatment was effective in reducing plasma membrane filipin staining without changing the punctate staining pattern (Supplemental Figure 5E). The reduced total filipin fluorescence after MβCD treatment was measured by flow cytometry (Supplemental Figure 5F). Using this method, we verified that *SPNS1* KO cells have increased intracellular cholesterol relative to WT cells even in the basal state, with Torin1 treatment further increasing filipin staining in *SPNS1* KO cells (Figure 4, F and G).

To confirm lysosomal cholesterol accumulation in *SPNS1* KO cells, we performed lipidomic analysis on isolated lysosomes and observed a 2-fold increase in lysosomal unesterified cholesterol (Figure 4H). Similar results were obtained when we metabolically labelled cells with [^{14}C]-cholesterol and subjected the extracted lipids from isolated lysosomes to thin layer chromatography (Supplemental Figure 5, G and H). Lastly, we reanalyzed lipidomic data from our previous study on liver-specific *Spns1* knockdown mice(10) and found a large increase in cholesterol in both liver and isolated lysosomes from *Spns1* knockdown mouse liver (Figure 4I), indicating that such disturbance in lysosomal and cellular cholesterol homeostasis is also observed at the organ level.

To more specifically determine if *SPNS1* KO cells have defective lysosomal cholesterol egress, cells were delipidated overnight followed by LDL loading, which would deliver cholesterol and cholesteryl ester directly to lysosomes. Cells were either labelled with [^{14}C]-oleate to quantify [^{14}C]-CE synthesis or stained with filipin to quantify endolysosomal cholesterol. With this

approach we observed a ~20% reduction in incorporation of [^{14}C]-oleate into [^{14}C]-CE (Supplemental Figure 6A) as well as a significant increase in the intracellular punctate distribution of filipin staining in SPNS1 KO cells that was exacerbated by Torin1 treatment (Supplemental Figure 6, B and C). Collectively, these findings suggest that cholesterol accumulates in lysosomes of *SPNS1* KO cells due to reduced lysosomal cholesterol egress.

Given that cellular cholesterol is sequestered in lysosomes in *SPNS1* KO cell, we wondered if that would result in a deficiency of ER and plasma membrane cholesterol, especially in delipidated conditions when there are no exogenous sources of cholesterol. It was reported that mTORC1 activates SREBP2 by suppressing cholesterol trafficking from lysosomes to ER, while mTORC1 inhibition has the opposite effect by activating lysosomal cholesterol egress resulting in suppression of SREBP2 processing(39). We hypothesized that if *SPNS1* KO cells have reduced lysosomal cholesterol egress, then there should be a blunting of SREBP2 suppression under conditions where cholesterol egress is enhanced (Figure 4J). To examine this possibility, WT and *SPNS1* KO cells were cultured in medium supplemented with delipidated fetal bovine serum (FBS) overnight to upregulate SREBP2 activity, followed by adding back FBS and Torin1 to stimulate the egress of cholesterol from lysosome to the ER. Under these experimental conditions *SPNS1* KO cells had an increased mature form of SREBP2 (nuclear-SREBP2) relative to WT cells (Figure 4K). To further validate this observation, we utilized a classic Sterol Response Element (SRE) luciferase reporter assay to quantify the transcriptional activity of SREBP. Consistent with increased SREBP2 processing, SREBP activity in *SPNS1* KO was elevated relative to WT cells (Figure 4L). We further confirmed this finding with RT-qPCR which showed upregulation of several classical SREBP2 target genes, namely *HMGCR* and *HMGCS*, in *SPNS1* KO cells relative to WT cells (Figure 4M). It is notable that *SPNS1* KO cells exposed to delipidated media already had elevated SREBP activity relative to WT cells (Supplemental Figure 6D), further suggesting that the *SPNS1* KO cells have reduced ER cholesterol. Together, these findings support the conclusion that SPNS1 deficiency results in a defect in lysosomal cholesterol egress.

The accumulation of ether-LPC and ether-LPE impedes lysosomal cholesterol egress

As the accumulation of LPC and cholesterol in lysosomes of *SPNS1* KO cells was further increased by mTOR inhibition (Figure 2A, Figure 4D, Supplemental Figure 5, B-D), we sought to test whether there exists a causal relationship between lysosomal LPC levels and cholesterol accumulation. We utilized PLA2G15, a lysosomal phospholipase A2 (PLA2) that also has phospholipase B (PLB) activity (8), to alter lysosomal LPC levels. PLA2G15 is reported to hydrolyze PC, PE, PG, PS, their corresponding lysophospholipids, and bis(monoacylglycerol)phosphate (BMP) in *in vitro* enzyme activity assays (8, 40). Therefore, PLA2G15 could either decrease or increase lysosomal LPC levels depending on whether its PLA2 or PLB activity is predominant. We purified His-tagged PLA2G15 to homogeneity (Supplemental Figure 7, A and B) and supplemented the WT and *SPNS1* KO cells with PLA2G15 and performed lipidomic analysis. Consistent with previous reports(8), treating cells with purified PLA2G15 resulted in cellular uptake of the enzyme (Supplemental Figure 7C). Lipidomic analysis revealed that LPC, LPE and LPS with mono- or poly-unsaturated fatty acids were decreased with PLA2G15 treatment, while LPC, LPE and LPS containing saturated fatty acids remained unchanged or were slightly elevated (Figure 5A). These changes are consistent with PLA2G15 having PLA2 activity that hydrolyzes the mono- and polyunsaturated fatty acids which are usually esterified at the sn-2 position on the glycerol backbone. Interestingly, while the total LPC and LPE was either reduced or unchanged (Figure 5, A-C), the level of LPC and LPE containing ether or vinyl-ether bonds (LPC-O/P and LPE-P) were greatly elevated upon supplementation of PLA2G15 in *SPNS1* KO cells but not in WT cells (Figure 5, A, D and E). This suggests that PLA2G15 is specific to the phospholipid ester bond and does not possess etherase activity. Indeed, purified PLA2G15 was able to digest PC, LPC and plasmalogen containing PC (PC-P) to release FFA but was unable to hydrolyze LPC-P (Supplemental Figure 7D). In an attempt to reduce lysosomal LPC-O/P and LPC-P levels, we knocked out *PLA2G15* in *SPNS1* KO cells. However, double knockout cells did not have significant changes in either LPC/LPE or LPC-O/P and LPE-P levels (Figure 5, A-E), indicating

the existence of other phospholipases in lysosomes that can generate lysophospholipids in the absence of PLA2G15.

To determine the effect of reduced lysosomal LPC/LPE with increased LPC-O/P and LPE-P on lysosomal cholesterol, we quantified filipin staining using flow cytometry analysis. Intracellular filipin staining, as a marker for lysosomal cholesterol, was unchanged in WT cells with PLA2G15 supplementation but was significantly elevated in *SPNS1* KO cells in both basal and Torin1 treated conditions (Supplemental Figure 7E), a finding that was confirmed by lipidomic analysis (Figure 5F). The accumulation of cholesterol in *SPNS1* KO cells treated with PLA2G15 was unlikely due to reduction of BMP, a substrate of PLA2G15, because WT cells treated with PLA2G15 had a larger drop in BMP levels than *SPNS1* KO cells without changes in cholesterol levels (Figure 5A). Importantly, the total amount of lysophospholipids (LPC, LPC-O/P, LPE, LPE-P) was unchanged with PLA2G15 supplementation in KO cells (Figure 5G). Therefore, it is likely that the accumulation of LPC-O/P and LPE-P, but not LPC and LPE, is causative for lysosomal cholesterol egress defect in *SPNS1* KO cells.

Patient fibroblasts demonstrate a defect in cholesterol egress and neutral lipid synthesis under mTOR inhibition.

We next set out to test if patient fibroblasts with mutant *SPNS1* exhibited similar disturbances in cellular lipid homeostasis as found in *SPNS1* KO HEK293T cells. We first confirmed by filipin staining that patient fibroblasts, but not their age matched controls, accumulated cholesterol in lysosomes upon mTOR inhibition (Figure 6, A and B). We similarly used MβCD to deplete plasma membrane cholesterol and measured cellular lipid levels by lipidomic analysis. Torin1 treatment resulted in significantly increased levels of LPC and LPC-O in patient fibroblasts and to a much lower extent in controls, as well as a slight increase in cellular cholesterol level (Supplemental Figure 8). We next looked at the rate of neutral lipid synthesis upon placing cells in HBSS media to induce amino acid starvation, a condition that reduces mTOR activity. Both control and patient fibroblasts were able to increase synthesis of TAG and some classes of CE upon amino acid starvation, but the extent of increase was less in patient

fibroblasts (Figure 6, C and D). This data is consistent with our findings that LPC transported out of lysosomes by SPNS1 contributes fatty acid for TAG in LD biogenesis.

Discussion:

In this study, we identified two families with biallelic nonsynonymous variants in *SPNS1* that inactivate transporter function. The patients primarily presented with progressive muscle weakness, elevated creatinine, persistent elevation of liver transaminase and liver injury. The clinical presentation of the patients also showed similarities with phenotypes observed in mouse models of *Spns1* deficiency (10, 11, 15). We confirmed that the disease-causing mutations of *SPNS1* results in protein with reduced transport function or poorly expressed protein. We carried out in-depth characterization of lipidomic changes and cellular phenotypes using patients' fibroblasts from Family A with heterozygous mutations and confirmed elevation of LPC, LPE as well as other sphingolipid metabolites in patients' fibroblasts. This represents a lysosomal storage disease caused by *SPNS1* variants and defines a gene-disease association. It is notable that clinical phenotypes of our patients are different from the phenotypes of a previously reported single pedigree of three patients with a homozygous variant (p.Pro295Leu) of SPNS1 that presented mainly with neurological symptoms such as cerebellar defects and neurodevelopment delay, without liver and muscle involvement(11). We further characterized this variant and found that P295L was poorly expressed but fully complemented elevated LPCs in *SPNS1* KO cells. It would be important to determine if the p.Pro295Leu variant causes LPC accumulation in cells in order to confirm causation of disease in these patents. Nevertheless, it is possible that variants in *SPNS1* could lead to a spectrum of disease.

In the attempt to understand the pathogenesis of this newly characterized lysosomal storage disease, we discovered additional roles of SPNS1 in maintaining cellular lipid homeostasis other than phospholipid salvage. While lysosomal choline recycling might be important for cancer cell survival in choline deficient conditions (12), essential deficiency of choline is rare (13). *SPNS1* KO cells and animals do not have PC deficiency (10, 11). As such, it is unlikely

533 that the *SPNS1* patients' disease are caused by inefficient choline salvage from lysosomes.
534 Therefore, we sought to understand the full metabolic fate of LPC transported out of
535 lysosomes. While it has been shown that phospholipid synthesis is important for LD expansion
536 (41), and addition of exogenous LPC to cells can induce LD formation (42), direct evidence
537 for crosstalk between phospholipid catabolism and TAG synthesis was lacking. We provided
538 multiple lines of evidence that lysosomal LPC transported by SPNS1 quantitatively contributes
539 its fatty acid for TAG synthesis when mTOR activity is reduced, linking the catabolism of
540 lysosomal LPC to TAG synthesis and storage in cytosolic LD. The identity of the enzymes that
541 mediate the metabolism of LPC for TAG synthesis are not known. More recently,
542 TMEM68/DISEL has been identified as an alternative DGAT that generates TAG by potentially
543 utilizing membrane phospholipids as the fatty acyl donor (43, 44). It remains to be explored
544 whether TMEM68 can directly use lysosomal derived LPC, or PC derived from re-acylation of
545 lysosomal-derived LPC as substrate for TAG synthesis.

546 One of the more unexpected findings from our study was that SPNS1 deficiency led to a
547 reduction in lysosomal cholesterol egress that was due in part to accumulation of lysosomal
548 ether-LPC/LPE. Our experimental use of PLA2G15, a known lysosomal phospholipase,
549 allowed us to make compositional change of lysosomal lipidome without altering the total
550 amount of lysophospholipids. This method helped to pinpoint alkyl and vinyl ether LPC (LPC-
551 O/P) and LPE (LPE-P) as likely causative lipid species leading to reduced lysosomal
552 cholesterol egress in *SPNS1* KO cells. This effect was SPNS1 dependent because PLA2G15
553 supplementation in WT cells did not increase levels of LPC-O/P and LPE-P which are
554 substrates for SPNS1 transport (10). While it is possible that some of the lysosomal LPC and
555 LPE are hydrolyzed further to GPC and glycerophosphorylethanolamine (GPE) by PLA2G15
556 (8), our findings indicate that LPC-O/P and LPE-P are entirely reliant on SPNS1 to exit the
557 lysosome. Indeed, there is no reported lysoplasmalogenase activities in lysosomes. So far,
558 the only identified lysoplasmalogenase is TMEM86A/B that localizes to the ER (45, 46).
559 Therefore, a potential evolutionary role of SPNS1 could be for lysosomal LPC-O/P and LPE-

P transport and salvage. How LPC-O/P and LPE-P accumulation contributed to cholesterol accumulation is unknown. Interestingly, deficiency of cellular plasmalogen was shown to be associated with defects in cellular cholesterol trafficking and HDL mediated cholesterol efflux (47, 48). In fact, TMEM86A was reported to be regulated by sterol controlled-liver X receptor (49), further suggesting an association of cellular plasmalogen level and cholesterol trafficking. While LPC itself has been reported to form complexes with cholesterol in a 1:1 molar ratio in *in vitro* systems (50), the possibility remains to be tested that physical interactions between LPC-O/P and LPE-P and cholesterol, and potentially other accumulated lipids such as sphingosine and ceramide, impede cholesterol movement inside the lysosome. Alternatively, LPC-O/P and LPE-P may compete or affect the binding of cholesterol to NPC2 and NPC1. Edelfosine, a synthetic alkyl-lysophospholipid structurally similar to LPC-O, was shown to inhibit cholesterol binding to purified NPC2 and the N-terminus of NPC1 (51, 52). Reassuringly, when we performed data-mining on an existing CRISPR screen for regulators of cellular cholesterol by treating cells with a NPC1 inhibitor (53), we found that *SPNS1* emerged as a positive regulator of lysosomal cholesterol egress.

How might these lysosomal and cellular lipid changes contribute to the disease pathogenesis in *SPNS1* loss-of-function is less clear. While we did not observe any deficiency of PC or PE species in patient fibroblasts, we found a decrease in plasmalogen PC and PE with an associated increase in LPC-O/P and LPE-P (Figure 1I). It is tempting to speculate that lysosomal transport of LPC-O/P and LPE-P by SPNS1 forms an ether-phospholipid salvage pathway that could be physiologically important for maintaining cellular plasmalogens. Plasmalogens have diverse functions ranging from serving as a reservoir for signaling molecules, modulating membrane properties to being an antioxidant (54-56). Defective lysosomal cholesterol egress associated with lysosomal accumulation of LPC-O/P and LPE-P in SPNS1 deficiency is reminiscent of NPC1/2 disease and could be a contributing factor in causing disease in *SPNS1* patients. Other possible causes of disease in *SPNS1* patients could relate directly to reduced ability of cells to adapt to reduced amino acid availability, either

through reduced ability to store energy as TAG in LD and/or defective autophagy. LPC and LPE have detergent like properties that could lead to lysosomal dysfunction that could be exacerbated during nutrient starvation, when autophagy is important for clearance of damaged cellular organelles (57). A general defect in autophagy could lead to gradual accumulation of damaged organelles such as mitochondria which could be toxic to cell viability (58). Although LC3b-II levels were unchanged in patients' fibroblasts, we cannot rule out that autophagy is not affected in tissues in the *SPNS1* patients.

Taken together, our study reports a lysosomal storage disease resulting from inactivating mutations in *SPNS1* that revealed crosstalk between lysosomal lysophospholipid transport with the regulation of cellular cholesterol and TAG homeostasis.

Methods

Additional details can be found in Supplemental Data.

Sex as a biological variable

Our study examined two families with rare biallelic variants in *SPNS1*. Both sexes were examined that included three affected males, one female heterozygous carrier and one male heterozygous carrier.

Statistical analysis

Statistical analysis was performed using GraphPad PRISM using two-sided unpaired student's t test, and one-way and two-way ANOVA with Dunnett's test or with Turkey's test as indicated. The number of independent experiments for each figure were indicated in figures and in figure captions. All experiments were carried out in at least triplicates. Exact p-value for lipidomic analysis was reported in supplemental data sets. A P value less than 0.05 was considered significant.

Study Approval

The study on Family A was approved by the Regional Ethical Review Board in Stockholm, Sweden (ethics permit number 2019-04746) in accordance with the Declaration of Helsinki. Informed consent was obtained from the legal guardians. Study on Family B was approved by the local ethics committee of the Technical University Munich (5360/121 S). Both parents gave written informed consent and the study is conducted in compliance with the declaration of Helsinki.

Data availability

The patients' genomic data cannot be deposited in a public repository due to legal and ethical restrictions under Swedish, German, and EU regulations, including GDPR. Variant-level data (gene, HGVS, zygosity, inheritance, and population frequency) are provided in the manuscript. Further details may be available upon request to Ann Nordgren (ann.nordgren@ki.se), Helena Malmgren (helena.malmgren@ki.se), and Matias Wagner (Matias.Wagner@mri.tum.de) pending appropriate ethical approvals. Values for all data points in graphs are reported in the Supporting Data Values file. Lipidomics data are found in Supplemental data set.

Acknowledgements

We would like to thank all members of the family participating in this study. This work was supported by grants from the Ministry of Health, and Ministry of Education, Singapore (MOH-000217, MOH-001206, MOE-T2EP30220-0001, MOE2019-T2-1-031), Goh Cardiovascular Research Award (Duke-NUS-GCR/2025/0044), and SingHealth Duke-NUS Genomic Medicine Centre Seed Grant (SDDC/FY2023/EX/79-A117) to D. L. S., C. F. C is supported by MOH-001234. AN was supported by grants from the Swedish Childhood Cancer Fund (PR2022-0027), and Hållsten Research foundation. AN & TS was supported by Stockholm Regional Council (ALF funding). AN & MD was funded by the Swedish Research Council (2023-06393) and (2021-02860). TS was supported by grant from research fund to the Center

for Neuromusculoskeletal Restorative Medicine from Health@InnoHK program launched by Innovation and Technology Commission, the Government of the Hong Kong Special Administrative Region of the People's Republic of China. MCL is funded by a Walter Benjamin Fellowship of the German Research Foundation (Deutsche Forschungsgemeinschaft (DFG) – Project number 521414448)

The authors acknowledge support from the National Genomics Infrastructure in Stockholm funded by Science for Life Laboratory, the Knut and Alice Wallenberg Foundation and the Swedish Research Council, and SNIC/Uppsala Multidisciplinary Center for Advanced Computational Science for assistance with massively parallel sequencing and access to the UPPMAX computational infrastructure.

Several of the authors of this publication are members of the European Reference Network on Rare Congenital Malformations and Rare Intellectual Disability ERN-ITHACA [EU Framework Partnership Agreement ID: 3HP-HP-FPA ERN-01-2016/739516]. Funders had no role in study design, data collection and analysis, decision to publish, or preparation of the manuscript.

Graphical abstract and Figure 4J were created using Biorender with permission.

Author contributions

Conceptualization, M.H. and D.L.S.; methodology, M.H., F.T and D.L.S. ; investigation, M.H.; Genetic and Clinical analysis, M.E., H.M., M.C.V.M., V.A., M.D., A.D.V., T.S., A.N., M.W., M.C.L, J.H.; MS data acquisition and analysis, M.D., M.C., F.T.; supervision, D.L.S.; manuscript writing-original draft, M.H. and D.L.S.; all authors reviewed the manuscript and provided input; funding acquisition, D.L.S., F.T., C.F.C., A.N., T.S., M.D., M.C.L.

Reference:

1. Infante RE, Wang ML, Radhakrishnan A, Kwon HJ, Brown MS, and Goldstein JL. NPC2 facilitates bidirectional transfer of cholesterol between NPC1 and lipid bilayers, a step in cholesterol egress from lysosomes. *Proceedings of the National Academy of Sciences*. 2008;105(40):15287-92.

2. Millard EE, Gale SE, Dudley N, Zhang J, Schaffer JE, and Ory DS. The Sterol-sensing Domain of the Niemann-Pick C1 (NPC1) Protein Regulates Trafficking of Low Density Lipoprotein Cholesterol. *Journal of Biological Chemistry*. 2005;280(31):28581-90.
3. Carstea ED, Morris JA, Coleman KG, Loftus SK, Zhang D, Cummings C, et al. Niemann-Pick C1 Disease Gene: Homology to Mediators of Cholesterol Homeostasis. *Science*. 1997;277(5323):228-31.
4. Loftus SK, Morris JA, Carstea ED, Gu JZ, Cummings C, Brown A, et al. Murine Model of Niemann-Pick C Disease: Mutation in a Cholesterol Homeostasis Gene. *Science*. 1997;277(5323):232-5.
5. Verot L, Chikh K, Freydière E, Honoré R, Vanier MT, and Millat G. Niemann-Pick C disease: functional characterization of three NPC2 mutations and clinical and molecular update on patients with NPC2. *Clin Genet*. 2007;71(4):320-30.
6. Brown MS, and Goldstein JL. The SREBP Pathway: Regulation of Cholesterol Metabolism by Proteolysis of a Membrane-Bound Transcription Factor. *Cell*. 1997;89(3):331-40.
7. Radhakrishnan A, Sun L-P, Kwon HJ, Brown MS, and Goldstein JL. Direct Binding of Cholesterol to the Purified Membrane Region of SCAP: Mechanism for a Sterol-Sensing Domain. *Molecular Cell*. 2004;15(2):259-68.
8. Nyame K, Hims A, Aburous A, Laqtom NN, Dong W, Medoh UN, et al. Glycerophosphodiesters inhibit lysosomal phospholipid catabolism in Batten disease. *Molecular Cell*. 2024;84(7):1354-64.e9.
9. Shayman JA, and Tesmer JJG. Lysosomal phospholipase A2. *Biochimica et Biophysica Acta (BBA) - Molecular and Cell Biology of Lipids*. 2019;1864(6):932-40.
10. He M, Kuk ACY, Ding M, Chin CF, Galam DLA, Nah JM, et al. Spns1 is a lysophospholipid transporter mediating lysosomal phospholipid salvage. *Proceedings of the National Academy of Sciences*. 2022;119(40):e2210353119.
11. Ha HTT, Liu S, Nguyen XTA, Vo LK, Leong NCP, Nguyen DT, et al. Lack of SPNS1 results in accumulation of lysolipids and lysosomal storage disease in mouse models. *JCI Insight*. 2024;9(8).
12. Scharenberg SG, Dong W, Ghoochani A, Nyame K, Levin-Konigsberg R, Krishnan AR, et al. An SPNS1-dependent lysosomal lipid transport pathway that enables cell survival under choline limitation. *Science Advances*. 2023;9(16):eadf8966.
13. Kenny TC, Khan A, Son Y, Yue L, Heissel S, Sharma A, et al. Integrative genetic analysis identifies FLVCR1 as a plasma-membrane choline transporter in mammals. *Cell Metabolism*. 2023;35(6):1057-71.e12.
14. Ichimura Y, Sugiura Y, Katsuragi Y, Sou Y-S, Uemura T, Tamura N, et al.: eLife Sciences Publications, Ltd; 2024.
15. Zhang X, Zhang F, Wu H, Yu Z, and Zhuang C. SPNS1 ablation drives skeletal muscle atrophy by disrupting mitophagy, mitochondrial function, and apoptosis in mice. *Genes & Diseases*. 2024;11(5):101083.
16. Sasaki T, Lian S, Khan A, Llop JR, Samuelson AV, Chen W, et al. Autolysosome biogenesis and developmental senescence are regulated by both Spns1 and v-ATPase. *Autophagy*. 2017;13(2):386-403.

17. Rong Y, McPhee CK, Deng S, Huang L, Chen L, Liu M, et al. Spinster is required for autophagic lysosome reformation and mTOR reactivation following starvation. *Proceedings of the National Academy of Sciences*. 2011;108(19):7826-31.
18. Laplante M, and Sabatini DM. An Emerging Role of mTOR in Lipid Biosynthesis. *Current Biology*. 2009;19(22):R1046-R52.
19. Saxton RA, and Sabatini DM. mTOR Signaling in Growth, Metabolism, and Disease. *Cell*. 2017;168(6):960-76.
20. Wullschleger S, Loewith R, and Hall MN. TOR Signaling in Growth and Metabolism. *Cell*. 2006;124(3):471-84.
21. Hosios AM, Wilkinson ME, McNamara MC, Kalafut KC, Torrence ME, Asara JM, et al. mTORC1 regulates a lysosome-dependent adaptive shift in intracellular lipid species. *Nature Metabolism*. 2022;4(12):1792-811.
22. Schmidt A, Danyel M, Grundmann K, Brunet T, Klinkhammer H, Hsieh T-C, et al. Next-generation phenotyping integrated in a national framework for patients with ultrarare disorders improves genetic diagnostics and yields new molecular findings. *Nature Genetics*. 2024;56(8):1644-53.
23. Braulke T, and Bonifacino JS. Sorting of lysosomal proteins. *Biochimica et Biophysica Acta (BBA) - Molecular Cell Research*. 2009;1793(4):605-14.
24. Boren J, and Brindle KM. Apoptosis-induced mitochondrial dysfunction causes cytoplasmic lipid droplet formation. *Cell Death & Differentiation*. 2012;19(9):1561-70.
25. Gubern A, Barceló-Torns M, Casas J, Barneda D, Masgrau R, Picatoste F, et al. Lipid Droplet Biogenesis Induced by Stress Involves Triacylglycerol Synthesis That Depends on Group VIA Phospholipase A_2. *Journal of Biological Chemistry*. 2009;284(9):5697-708.
26. Hapala I, Marza E, and Ferreira T. Is fat so bad? Modulation of endoplasmic reticulum stress by lipid droplet formation. *Biology of the Cell*. 2011;103(6):271-85.
27. Rambold Angelika S, Cohen S, and Lippincott-Schwartz J. Fatty Acid Trafficking in Starved Cells: Regulation by Lipid Droplet Lipolysis, Autophagy, and Mitochondrial Fusion Dynamics. *Developmental Cell*. 2015;32(6):678-92.
28. Nguyen TB, Louie SM, Daniele JR, Tran Q, Dillin A, Zoncu R, et al. DGAT1-Dependent Lipid Droplet Biogenesis Protects Mitochondrial Function during Starvation-Induced Autophagy. *Developmental Cell*. 2017;42(1):9-21.e5.
29. Nguyen LN, Ma D, Shui G, Wong P, Cazenave-Gassiot A, Zhang X, et al. Mfsd2a is a transporter for the essential omega-3 fatty acid docosahexaenoic acid. *Nature*. 2014;509(7501):503-6.
30. Cater RJ, Chua GL, Erramilli SK, Keener JE, Choy BC, Tokarz P, et al. Structural basis of omega-3 fatty acid transport across the blood–brain barrier. *Nature*. 2021;595(7866):315-9.
31. Nnah IC, Wang B, Saqcena C, Weber GF, Bonder EM, Bagley D, et al. TFEB-driven endocytosis coordinates MTORC1 signaling and autophagy. *Autophagy*. 2019;15(1):151-64.
32. Zhou J, Tan S-H, Nicolas V, Bauvy C, Yang N-D, Zhang J, et al. Activation of lysosomal function in the course of autophagy via mTORC1 suppression and autophagosome-lysosome fusion. *Cell Research*. 2013;23(4):508-23.

33. Sandhu J, Li S, Fairall L, Pfisterer SG, Gurnett JE, Xiao X, et al. Aster Proteins Facilitate Nonvesicular Plasma Membrane to ER Cholesterol Transport in Mammalian Cells. *Cell*. 2018;175(2):514-29.e20.
34. Horenkamp FA, Valverde DP, Nunnari J, and Reinisch KM. Molecular basis for sterol transport by StART-like lipid transfer domains. *The EMBO Journal*. 2018;37(6):e98002.
35. Infante RE, and Radhakrishnan A. Continuous transport of a small fraction of plasma membrane cholesterol to endoplasmic reticulum regulates total cellular cholesterol. *eLife*. 2017;6:e25466.
36. Chakravarthy BR, Spence MW, Clarke JTR, and Cook HW. Rapid isolation of neuroblastoma plasma membranes on Percoll gradients. Characterization and lipid composition. *Biochimica et Biophysica Acta (BBA) - Biomembranes*. 1985;812(1):223-33.
37. Lange Y, Strebel F, and Steck TL. Role of the plasma membrane in cholesterol esterification in rat hepatoma cells. *Journal of Biological Chemistry*. 1993;268(19):13838-43.
38. Zidovetzki R, and Levitan I. Use of cyclodextrins to manipulate plasma membrane cholesterol content: evidence, misconceptions and control strategies. *Biochim Biophys Acta*. 2007;1768(6):1311-24.
39. Eid W, Dauner K, Courtney KC, Gagnon A, Parks RJ, Sorisky A, et al. mTORC1 activates SREBP-2 by suppressing cholesterol trafficking to lysosomes in mammalian cells. *Proceedings of the National Academy of Sciences*. 2017;114(30):7999-8004.
40. Abe A, Hinkovska-Galcheva V, Bouchev P, Bouley R, and Shayman JA. The role of lysosomal phospholipase A2 in the catabolism of bis(monoacylglycerol)phosphate and association with phospholipidosis. *Journal of Lipid Research*. 2024;65(7).
41. Krahmer N, Guo Y, Wilfling F, Hilger M, Lingrell S, Heger K, et al. Phosphatidylcholine Synthesis for Lipid Droplet Expansion Is Mediated by Localized Activation of CTP:Phosphocholine Cytidylyltransferase. *Cell Metabolism*. 2011;14(4):504-15.
42. Lee J, and Ridgway ND. Phosphatidylcholine synthesis regulates triglyceride storage and chylomicron secretion by Caco2 cells. *Journal of Lipid Research*. 2018;59(10):1940-50.
43. McLelland G-L, Lopez-Osias M, Verzijl CRC, Ellenbroek BD, Oliveira RA, Boon NJ, et al. Identification of an alternative triglyceride biosynthesis pathway. *Nature*. 2023;621(7977):171-8.
44. Wang Y, Zeng F, Zhao Z, He L, He X, Pang H, et al. *International Journal of Molecular Sciences*. 2023.
45. Cho YK, Yoon YC, Im H, Son Y, Kim M, Saha A, et al. Adipocyte lysoplasmalogenase TMEM86A regulates plasmalogen homeostasis and protein kinase A-dependent energy metabolism. *Nature Communications*. 2022;13(1):4084.
46. Wu LC, Pfeiffer DR, Calhoon EA, Madiai F, Marcucci G, Liu S, et al. Purification, identification, and cloning of lysoplasmalogenase, the enzyme that catalyzes hydrolysis of the vinyl ether bond of lysoplasmalogen. *J Biol Chem*. 2011;286(28):24916-30.

47. Mandel H, Sharf R, Berant M, Wanders RJA, Vreken P, and Aviram M. Plasmalogen Phospholipids Are Involved in HDL-Mediated Cholesterol Efflux: Insights from Investigations with Plasmalogen-Deficient Cells. *Biochemical and Biophysical Research Communications*. 1998;250(2):369-73.
48. Munn NJ, Arnio E, Liu D, Zoeller RA, and Liscum L. Deficiency in ethanolamine plasmalogen leads to altered cholesterol transport. *Journal of Lipid Research*. 2003;44(1):182-92.
49. van Wouw SAE, van den Berg M, El Ouraoui M, Meurs A, Kingma J, Ottenhoff R, et al. Sterol-regulated transmembrane protein TMEM86a couples LXR signaling to regulation of lysoplasmalogens in macrophages. *Journal of Lipid Research*. 2023;64(2).
50. Ramsammy LS, and Brockerhoff H. Lysophosphatidylcholine-cholesterol complex. *Journal of Biological Chemistry*. 1982;257(7):3570-4.
51. Winkler MBL, Kidmose RT, Szomek M, Thaysen K, Rawson S, Muench SP, et al. Structural Insight into Eukaryotic Sterol Transport through Niemann-Pick Type C Proteins. *Cell*. 2019;179(2):485-97.e18.
52. Nel L, Thaysen K, Jamecna D, Olesen E, Szomek M, Langer J, et al. Structural and biochemical analysis of ligand binding in yeast Niemann–Pick type C1–related protein. *Life Science Alliance*. 2024;8(1):e202402990.
53. Lu A, Hsieh F, Sharma BR, Vaughn SR, Enrich C, and Pfeffer SR. CRISPR screens for lipid regulators reveal a role for ER-bound SNX13 in lysosomal cholesterol export. *Journal of Cell Biology*. 2021;221(2):e202105060.
54. Thai T-P, Rodemer C, Jauch A, Hunziker A, Moser A, Gorgas K, et al. Impaired membrane traffic in defective ether lipid biosynthesis. *Human Molecular Genetics*. 2001;10(2):127-36.
55. Zoeller RA, Lake AC, Nagan N, Gaposchkin DP, Legner MA, and Lieberthal W. Plasmalogens as endogenous antioxidants: somatic cell mutants reveal the importance of the vinyl ether. *Biochemical Journal*. 1999;338(3):769-76.
56. Dorninger F, Forss-Petter S, Wimmer I, and Berger J. Plasmalogens, platelet-activating factor and beyond – Ether lipids in signaling and neurodegeneration. *Neurobiology of Disease*. 2020;145:105061.
57. Mizushima N. Autophagy: process and function. *Genes Dev*. 2007;21(22):2861-73.
58. Youle RJ, and Narendra DP. Mechanisms of mitophagy. *Nature Reviews Molecular Cell Biology*. 2011;12(1):9-14.

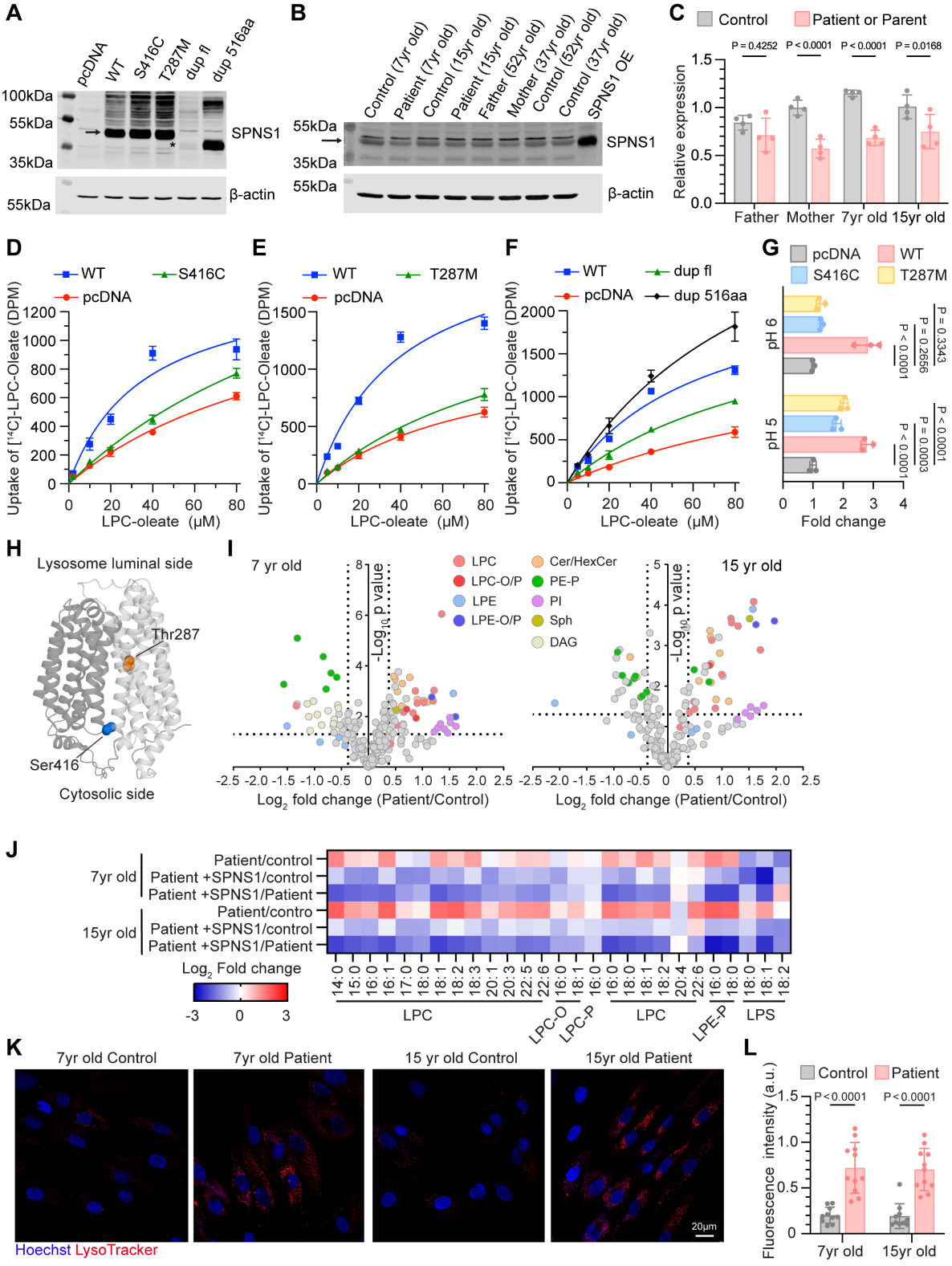
A
pcDNA
WT
S416C
T287M
dup fl
dup 516aa
100kDa
55kDa
35kDa
SPNS1
β-actin
B
Control (7yr old)
Patient (7yr old)
Control (15yr old)
Patient (15yr old)
Father (52yr old)
Mother (37yr old)
Control (52yr old)
Control (37yr old)
SPNS1 OE
C
Control
Patient or Parent
P = 0.4252
P < 0.0001
P < 0.0001
P = 0.0168
Relative expression
Father
Mother
7yr old
15yr old
D
WT
S416C
pcDNA
Uptake of [14C]-LPC-Oleate (DPM)
LPC-oleate (μM)
E
WT
T287M
pcDNA
F
WT
dup fl
pcDNA
dup 516aa
G
pcDNA
WT
S416C
T287M
pH 6
pH 5
P = 0.3343
P < 0.0001
P = 0.2656
P < 0.0001
P = 0.0003
Fold change
H
Lysosome luminal side
Thr287
Ser416
Cytosolic side
I
7 yr old
15 yr old
LPC
LPC-O/P
LPE
LPE-O/P
Cer/HexCer
PE-P
PI
Sph
DAG
-Log10 p value
Log2 fold change (Patient/Control)
J
7yr old
15yr old
Patient/control
Patient +SPNS1/control
Patient +SPNS1/Patient
Log2 Fold change
LPC
LPC-O
LPC-P
LPE-P
LPS
K
7yr old Control
7yr old Patient
15 yr old Control
15yr old Patient
Hoechst LysoTracker
20μm
L
Control
Patient
P < 0.0001
P < 0.0001
Fluorescence intensity (a.u.)
7yr old
15yr old

Figure 1. Characterization of SPNS1 mutations identified in patient.

(**A**) Immunoblotting of ectopically expressed wild-type SPNS1 (WT), p.Ser416Cys (S416C), p.Thr287Met (T287M), c.143_146dupAGCG (dup fl) and duplication mutant starting from the alternative ATG (dup 516aa) in HEK293 cell. The arrow indicates SPNS1. Asterisk indicates the dup 516aa SPNS1 that migrates at lower molecular weight. (**B**) Immunoblotting of endogenous SPNS1 from patients' and parents' fibroblast cells with their respective age-matched controls. Cell lysate from HEK293 cells overexpressing wild-type SPNS1 (SPNS1 OE) was used as control. The arrow indicates SPNS1. (**C**) Quantification of SPNS1 protein level normalized to β actin in (**B**). (**D**)-(**F**) Concentration dependent transport of [^{14}C]-LPC-oleate by HEK293 cells overexpressing S416C (**D**), T287M (**E**), dup fl and dup 516aa (**F**) as compared to overexpressing WT and vector control (pcDNA) over 30 minutes at pH=6 extracellular buffer. (**G**) [^{14}C]-LPC-oleate transport activity of WT and mutant SPNS1 at pH=6 and pH=5. (**H**) Alpha-fold model of SPNS1 with Ser416 and Thr287 residues highlighted. (**I**) Volcano plot showing lipidomic changes of patient fibroblasts relative to their age-matched controls. Lipids are color-coded based on lipid species. (**J**) Heatmap representation of $\log_2$ transformed fold-change in lipid concentration for patient and their age-matched control fibroblasts transduced with lentivirus carrying either WT *SPNS1* construct or vector control. (**K**) LysoTracker staining of patient and control fibroblasts. Red: LysoTracker; Blue: Hoechst. Scale bar 20μm. (**L**) Quantification of LysoTracker fluorescence intensity of individual cell shown in (**K**) from at least 10 cells from five different images. Each data point represents one cell. n=4 replicates for (**C**) and n=3 replicates for (**D**)-(**G**), (**I**), (**J**). Data are represented as mean ± S.D. Statistical tests are two-sided unpaired t-test for (**I**) and (**J**), two-way ANOVA with Šídák's test for (**C**) and (**L**), and two-way ANOVA with Dunnett's test for (**G**). P values for (**I**) and (**J**) are presented in Supplemental Data.

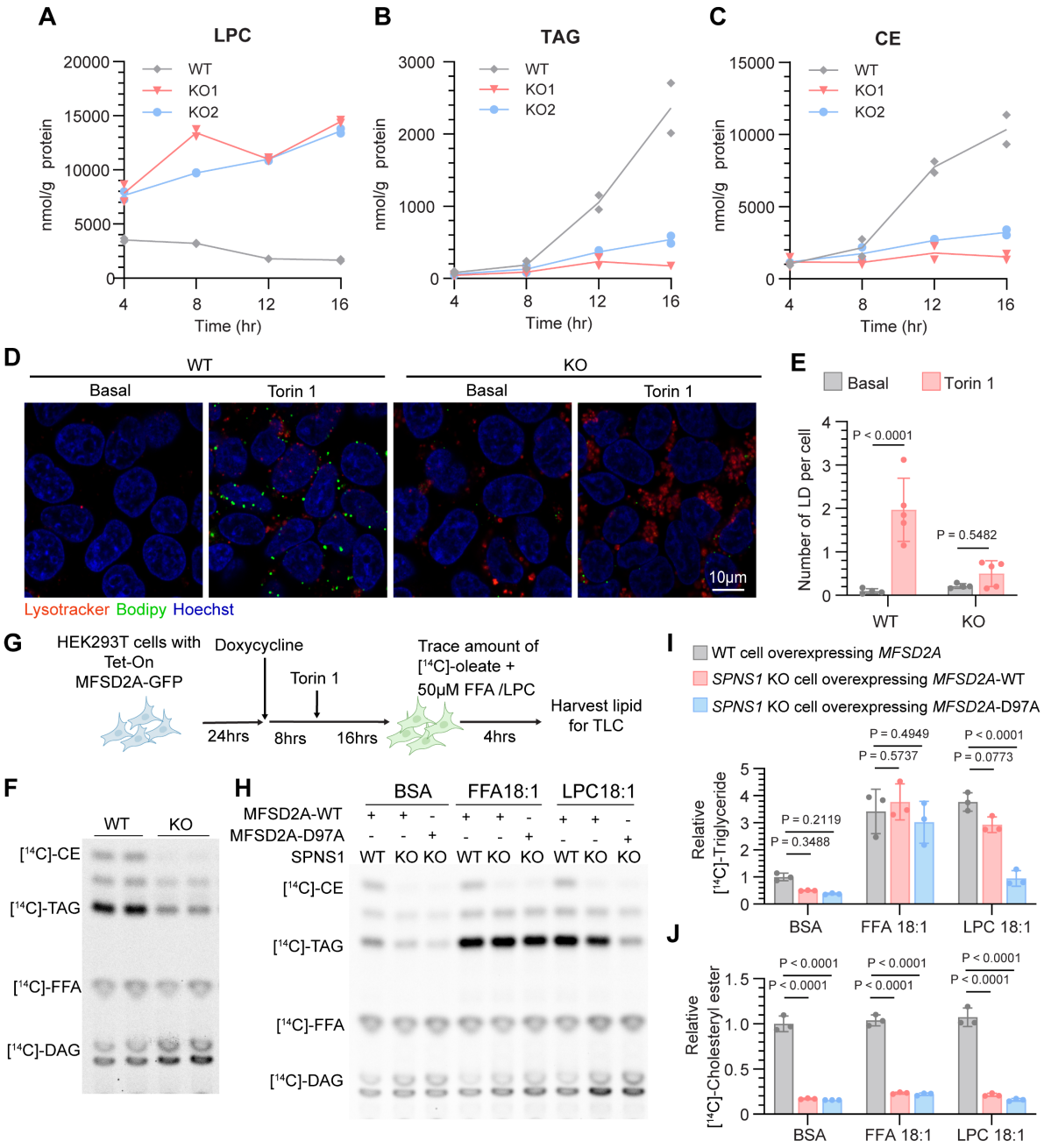

871

872

873

874

Figure 2. SPNS1 deficiency results in a defect in triglyceride and cholesteryl ester synthesis when mTOR activity is low.

(**A**)-(**C**) HEK293T WT and *SPNS1* KO cells were treated with 250 nM Torin1 and harvested at indicated timepoints for lipidomic analysis. Concentrations of total lyso-phosphatidylcholine (LPC) (**A**), TAG (**B**), and CE (**C**) were plotted over time. Two replicates per time point. (**D**) HEK293T WT and *SPNS1* KO cells were treated with or without 250 nM Torin1 for 16 hrs. Lipid droplets (LDs) were stained with BODIPY 493/503 (Green), and lysosomes were labelled with LysoTracker (Red). Blue: Hoechst. Scale bar 10μm. (**E**) Quantification of average number of LDs per cell in each field in (**D**). Each data point represents one field and five fields were scored for each condition. (**F**) HEK293T WT and *SPNS1* KO cells were treated with 250 nM Torin1 for 16 hrs then metabolically labelled with a trace amount of [^{14}C]-oleate (FFA) for 4 hrs. Formation of [^{14}C]-CE, [^{14}C]-TAG, and [^{14}C]-DAG were shown on TLC. (**G**) Schematic representation of radioisotope tracing study for (**H**)-(**J**). HEK293T WT and *SPNS1* KO cells harbouring doxycycline inducible *MFSD2A*-WT-GFP or *MFSD2A*-D97A-GFP (transport inactive mutant) were seeded for 24 hrs before treatment of 1 μg/ml doxycycline for 16 hrs. 250 nM Torin1 was added 8 hrs post doxycycline treatment and incubated for another 16 hrs. Cells were metabolically labelled with a trace amount of [^{14}C]-oleate together with 50 μM of FFA-18:1, LPC-18:1, or fatty acid free BSA for 4 hrs. Lipids were extracted from cells and analysed by TLC. (**H**) Representative TLC resolving [^{14}C]-labelled neutral lipid species. (**I**)(**J**) Quantification of [^{14}C]-TAG and [^{14}C]-CE bands from TLC analysis in (**H**) after normalized to protein concentration of each sample; n=3. Data are represented as mean ± S.D. Statistical tests are two-way ANOVA with Šídák's test for (**E**), and two-way ANOVA with Dunnett's for (**I**) and (**J**) for each treatment group.

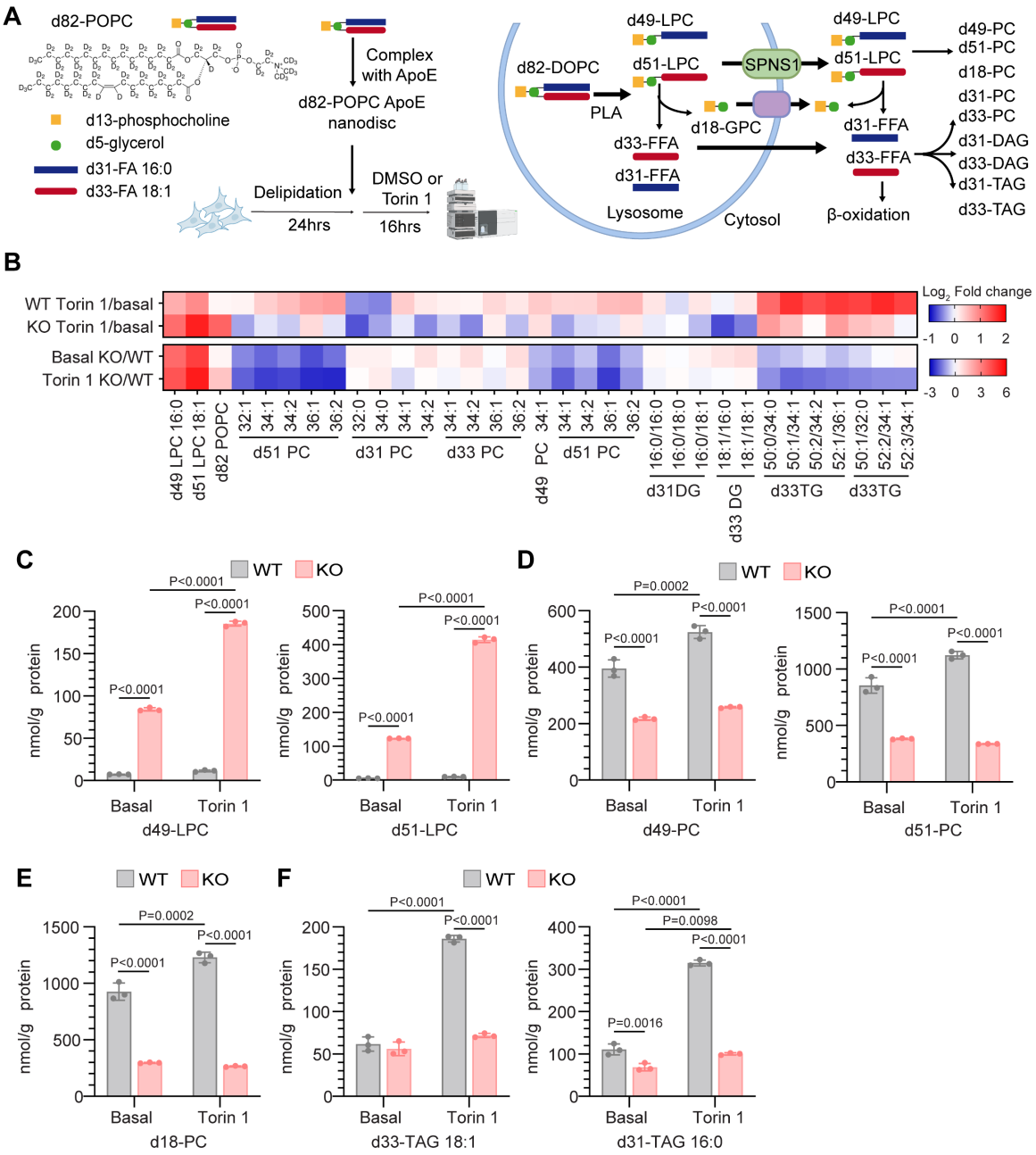
A
d82-POPC
d13-phosphocholine
d5-glycerol
d31-FA 16:0
d33-FA 18:1
Complex with ApoE
d82-POPC ApoE nanodisc
Delipidation
24hrs
DMSO or Torin 1
16hrs
d82-DOPC
PLA
d49-LPC
d51-LPC
d33-FFA
d31-FFA
Lysosome
SPNS1
d18-GPC
Cytosol
d49-PC
d51-PC
d18-PC
d31-PC
d33-PC
d31-DAG
d33-DAG
d31-TAG
d33-TAG
β-oxidation
B
WT Torin 1/basal
KO Torin 1/basal
Basal KO/WT
Torin 1 KO/WT
Log2 Fold change
d49 LPC 16:0
d51 LPC 18:1
d82 POPC
d51 PC
d31 PC
d33 PC
d49 PC
d31DG
d33 DG
d33TG
C
WT
KO
nmol/g protein
Basal
Torin 1
d49-LPC
d51-LPC
D
d49-PC
d51-PC
E
d18-PC
F
d33-TAG 18:1
d31-TAG 16:0

Figure 3. The fatty acyl moiety of LPC transported by SPNS1 contributes to triglyceride synthesis.

(**A**) Structure of d82-POPC (1-palmitoyl-2-oleoyl-glycero-3-phosphocholine) is shown together with the schematic representation of the experimental setup for the stable isotope tracing study for (**B**)-(**F**). The illustration on the right shows the catabolism of d82-POPC in lysosomes and potential metabolic fates of the GPC headgroup and fatty acyl tails. (**B**) Heatmap representation of the log_2 transformed concentration of lipid species in WT cells treated with Torin1 compared to untreated (WT Torin1/basal), *SPNS1* KO cells treated with Torin1 compared to untreated (KO Torin1/basal), KO cells compared to WT cells both at basal condition (Basal KO/WT), and KO cells compared to WT cells both with Torin1 treatment (Torin1 KO/WT); n=3 replicates. P-values were calculated using two tailed unpaired t-tests and are presented in Supplemental Data. (**C**)-(**F**) Concentration of per-deuterated LPC (d49-LPC, d51-LPC), sum of PC having labelled GPC with one labelled fatty acid (d49-PC, d51-PC), PC having labelled GPC (d18-PC), and TAG containing one labelled fatty acid (d31-TAG, d31-TAG); n=3 replicates. Data are represented as mean ± S.D. Statistical tests were two-way ANOVA with Tukey's test.

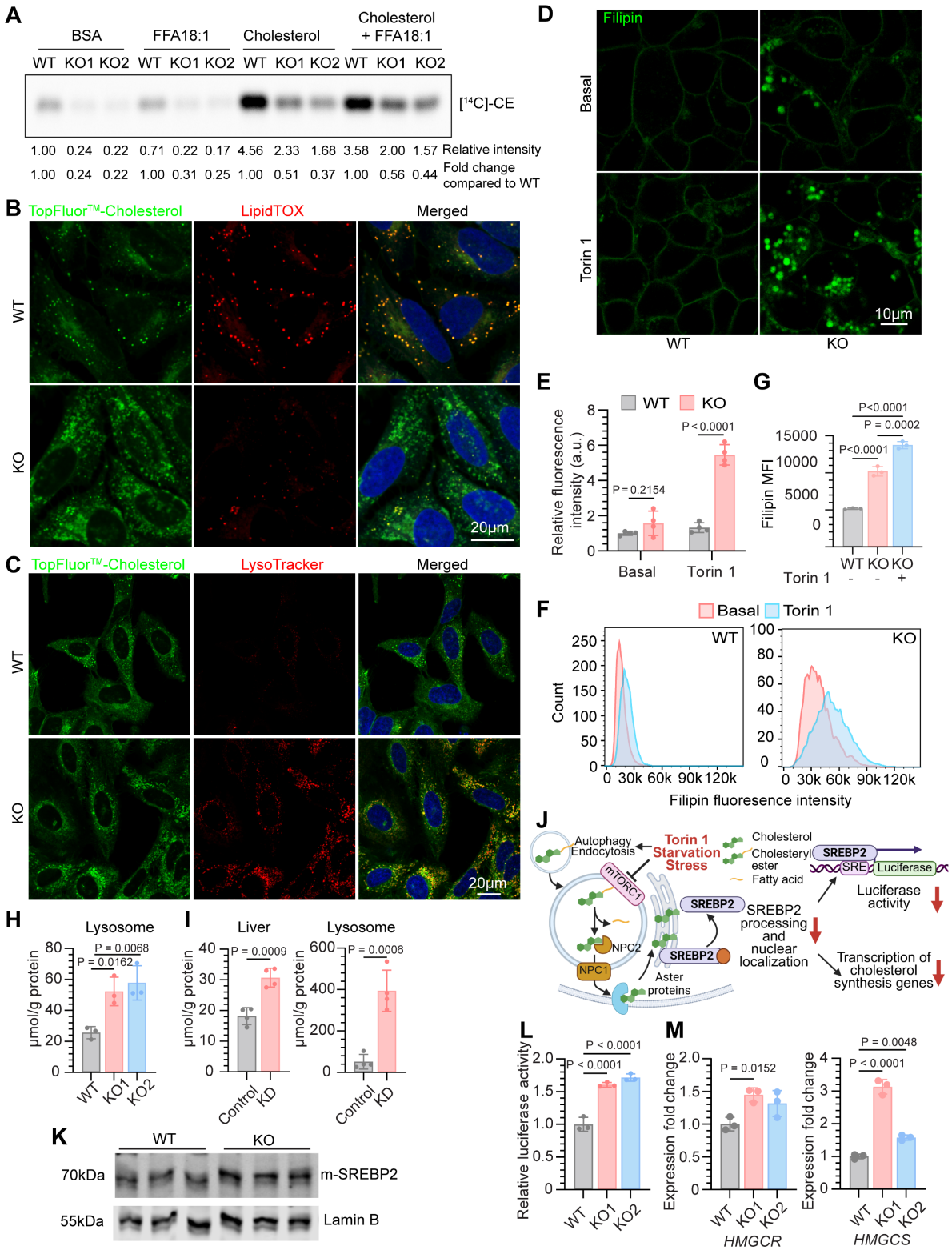
A
BSA
FFA18:1
Cholesterol
Cholesterol + FFA18:1
WT KO1 KO2 WT KO1 KO2 WT KO1 KO2 WT KO1 KO2
[14C]-CE
1.00 0.24 0.22 0.71 0.22 0.17 4.56 2.33 1.68 3.58 2.00 1.57 Relative intensity
1.00 0.24 0.22 1.00 0.31 0.25 1.00 0.51 0.37 1.00 0.56 0.44 Fold change compared to WT
B
TopFluor™-Cholesterol
LipidTOX
Merged
WT
KO
20μm
C
TopFluor™-Cholesterol
LysoTracker
Merged
WT
KO
20μm
D
Filipin
Basal
Torin 1
WT
KO
10μm
E
WT
KO
Relative fluorescence intensity (a.u.)
P = 0.2154
P < 0.0001
Basal
Torin 1
G
P<0.0001
P = 0.0002
P<0.0001
Filipin MFI
WT KO KO
Torin 1 - - +
F
Basal
Torin 1
WT
KO
Count
Filipin fluoresence intensity
J
Autophagy Endocytosis
Torin 1 Starvation Stress
mTORC1
Cholesterol
Cholesteryl ester
Fatty acid
SREBP2
SRE
Luciferase
Luciferase activity
SREBP2 processing and nuclear localization
Transcription of cholesterol synthesis genes
NPC2
NPC1
Aster proteins
H
Lysosome
P = 0.0068
P = 0.0162
μmol/g protein
WT KO1 KO2
I
Liver
P = 0.0009
Lysosome
P = 0.0006
μmol/g protein
Control KD
K
WT
KO
70kDa
m-SREBP2
55kDa
Lamin B
L
P < 0.0001
P < 0.0001
Relative luciferase activity
WT KO1 KO2
M
P = 0.0152
Expression fold change
HMGCR
P = 0.0048
P < 0.0001
Expression fold change
HMGCS
WT KO1 KO2

Figure 4. SPNS1 KO cells have defective lysosomal cholesterol egress.

(**A**) Quantification of CE synthesis in HEK293T WT and *SPNS1* KO cells. After 16 hrs of Torin1 treatment, a trace amount of [^{14}C]-oleate with fatty acid free BSA, or 20 μM of FFA-18:1, or 35.7 μM cholesterol-MβCD complex or 20 μM of FFA-18:1 and 35.7 μM cholesterol-MβCD complex were added to cells for 4 hrs. Fold-change of [^{14}C]-CE band intensity relative to WT (BSA) or WT for each treatment group was calculated. (**B**) *SPNS1* KO and WT HeLa cells were labelled with TopFluor™-Cholesterol (Green) for 24 hrs followed by 16 hrs treatment with Torin1. Fixed cells were stained with LipidTOX™ (red) for LD. Scale bar: 20μm. (**C**) Live cell imaging of HeLa *SPNS1* KO and WT cells pulse-labelled with TopFluor™-Cholesterol (Green) complexed with MβCD, followed by 16 hrs treatment with Torin1. Blue: Hoechst. Scale bar = 20μm. (**D**) Filipin staining of HEK293T WT and *SPNS1* KO cells treated with or without Torin1. Scale bar =10μm. (**E**) Quantification of filipin staining fluorescence intensity in each field in (**D**). Four different fields were scored for each condition. (**F**) Representative flow cytometry profile of filipin intensity of HEK293T WT and *SPNS1* KO cells treated with or without Torin1. Plasma membrane cholesterol was depleted using MβCD before filipin staining. (**G**) Mean fluorescence intensity of filipin staining measured by flow cytometry in (**F**); n=3 replicates. (**H**) Concentration of lysosomal cholesterol from HEK293T WT and *SPNS1* KO cells; n=3 replicates. (**I**) Cholesterol levels in lysosomes and liver tissue from mice injected with AAV8 carrying shRNA targeting *Spns1* (KD) or nontargeting shRNA (control), n=4 mice per group. (**J**) Schematic illustration of how mTOR regulates lysosomal cholesterol egress to supress activation of SREBP2. (**K**)-(**M**) HEK293T WT and *SPNS1* KO cells were delipidated for 16 hrs. 10% FBS and Torin1 were added for another 8 hrs before harvesting cells. (**K**) Immunoblotting of mature SREBP2 (m-SREBP2) and Lamin B in nuclear fractions. (**L**) Luciferase reporter assay for SREBP transcriptional activity. (**M**) mRNA expression of select SREBP2 target genes; n=3 replicates. Data are represented as mean ± S.D. Statistical tests were two-way ANOVA with Šídák's test for (**E**), one-way ANOVA with Tukey's test for (**G**), one-way ANOVA with Dunnett's test for (**H**), (**L**) and (**M**), and two tailed unpaired t-test for (**I**).

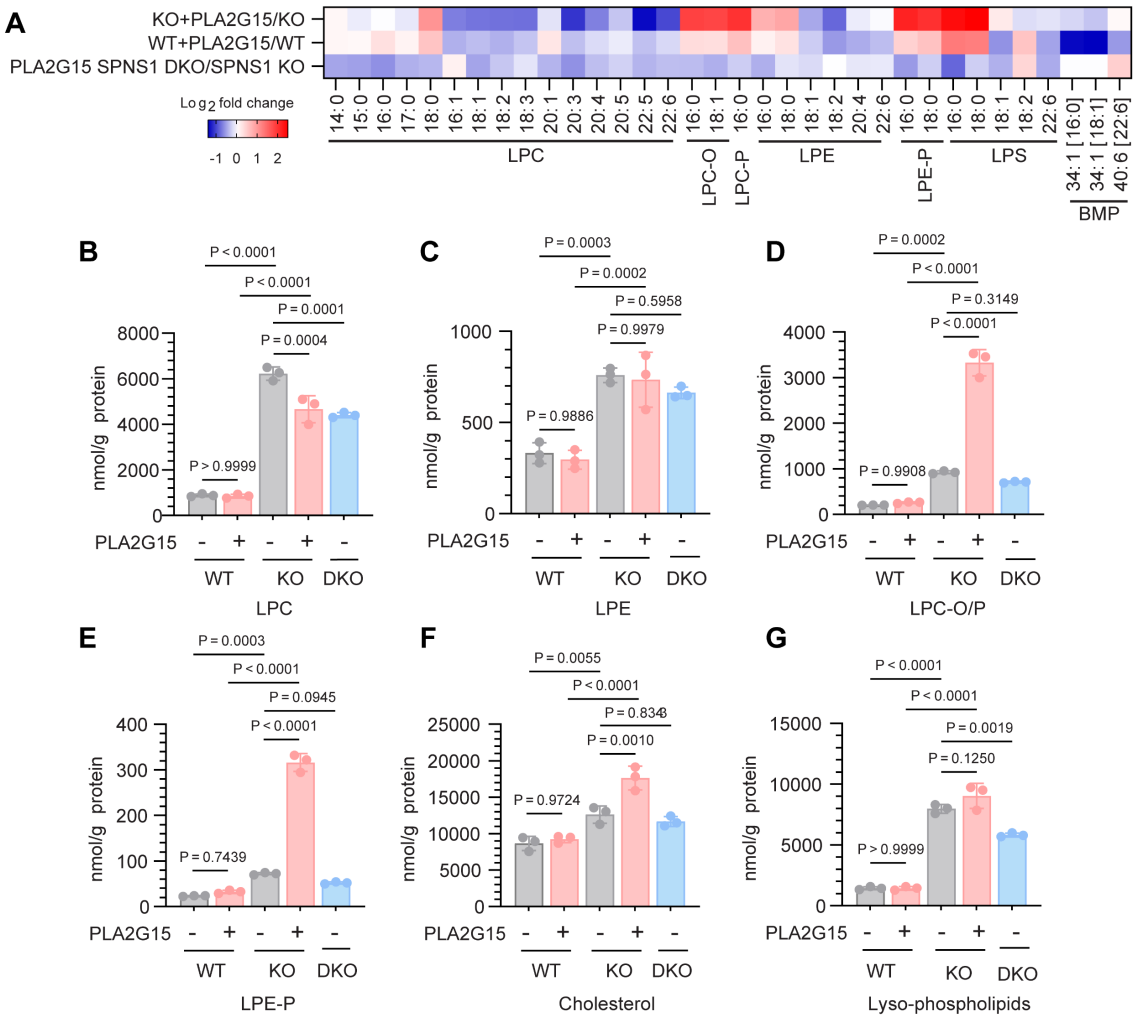

Figure 5. PLA2G15 enzyme supplementation increases lysosomal cholesterol.

HEK293T WT and *SPNS1* KO cells were supplemented with 3 μg/ml purified PLA2G15 for 48 hrs, and plasma membrane cholesterol was depleted using MβCD before harvesting for lipidomics analysis. (**A**) Heatmap representation of log_2 fold-change of lipid concentrations in *SPNS1* KO and WT with or without PLA2G15 supplementation, and *PLA2G15 SPNS1* double knockout (DKO) relative to *SPNS*1 KO cells. n=3 replicates; P-values were calculated using two-tailed unpaired t-tests and are presented in Supplemental Data. (**B**)-(**G**) Cellular concentrations of LPC, LPE, LPC-O/P, LPE-P, cholesterol, and sum of all lysophospholipids transported by SPNS1 (LPC, LPE, LPC-O/P, LPE-P). n=3 replicates. Data are represented as mean ± S.D. Statistical tests were one-way ANOVA with Šídák's test.

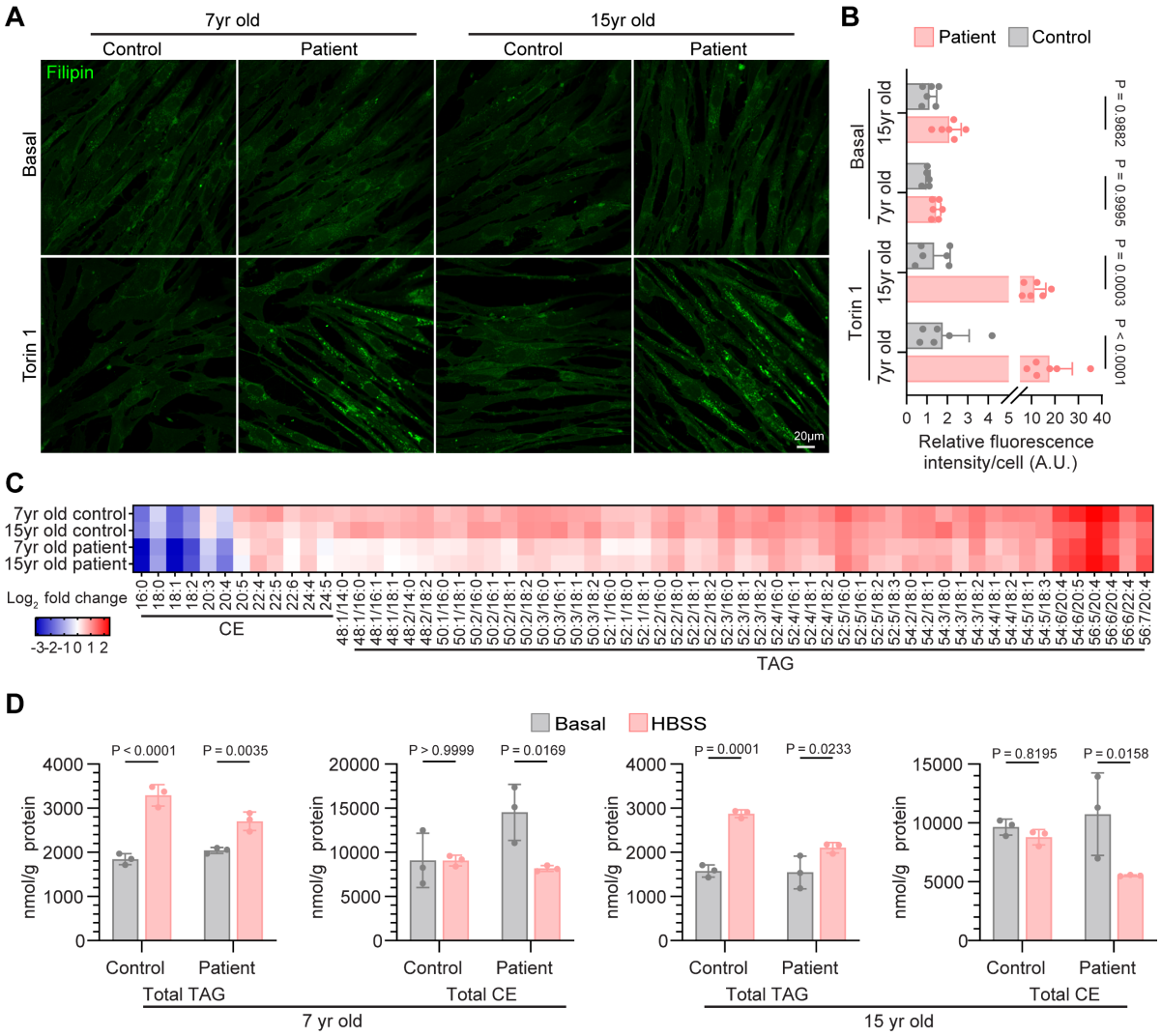

Figure 6. Fibroblasts from *SPNS1* patients have increased cholesterol and reduced neutral lipid synthesis under inhibition of mTOR.

(**A**) Filipin staining of patients' and age-matched controls' fibroblasts with or without 16 hrs of 250 nM Torin1 treatment. Scale bar =20μm (**B**) Quantification of filipin staining fluorescence intensity per cell in each field. Each data point represents one field and five different fields were scored. (**C**) Heatmap representation of $\log_2$ fold-change of neutral lipids species (CE and TAG) of each fibroblast cell line after 6 hrs of starvation in HBSS. P-values were calculated using two-tailed unpaired t-tests and are presented in Supplemental Data. (**D**) Concentration of total TAG and CE in patient fibroblasts and their age-matched control before and after HBSS treatment. n=3 replicates. Data are represented as mean ±S.D. Statistical tests were two-way ANOVA with Šídák's test for (**B**) and (**D**)..